Measurement of highly transient electrical charging following high-intensity laser–solid interaction

M. Borghesi[a] and L. Romagnani
Department of Pure and Applied Physics, The Queen's University of Belfast, Belfast BT7 1NN, United Kingdom

A. Schiavi,[b] D. H. Campbell, and M. G. Haines
The Blackett Laboratory, Imperial College, London SW7 1BZ, United Kingdom

O. Willi
Institut für Laser-und Plasmaphysik, Heinrich-Heine-Universität, Düsseldorf, Germany

A. J. Mackinnon
Lawrence Livermore National Laboratory, Livermore, California 94551

M. Galimberti and L. Gizzi
Istituto per i Processi Chimico-Fisici, CNR, Pisa, Italy

R. J. Clarke and S. Hawkes
Central Laser Facility, Rutherford Appleton Laboratory, Chilton OX11 0QX, United Kingdom

(Received 24 September 2002; accepted 23 January 2003)

The multi-million-electron-volt proton beams accelerated during high-intensity laser–solid interactions have been used as a particle probe to investigate the electric charging of microscopic targets laser-irradiated at intensity $\sim 10^{19}$ W cm^2. The charge-up, detected via the proton deflection with high temporal and spatial resolution, is due to the escape of energetic electrons generated during the interaction. The analysis of the data is supported by three-dimensional tracing of the proton trajectories. © *2003 American Institute of Physics.* [DOI: 10.1063/1.1560554]

During the interaction of ultraintense laser pulses with matter, a considerable fraction of the laser energy is converted into highly energetic charged particles.[1,2] In particular, beams of multi-million-electron-volt protons are generated during the interaction of ultraintense short pulses with thin solid targets.[2] These beams have exceptionally interesting properties (small source size, low divergence, short duration, large number density) with respect to application development.

Ion beams produced from conventional accelerator sources have been used in the past for radiographic applications[3] and for the detection of small amplitude electric fields in laser-produced plasmas.[4] Proton beams from ultraintense laser–foil interactions, by allowing two-dimensional (2-D) mapping with unprecedented spatial[5] and temporal resolution, advance enormously the potential of particle probing applications. Recently, their use as a particle probe has led to the observation of structures identified as remnants of post-solitons following relativistic laser–plasma interactions.[6] In this letter, the detection of highly transient electric charging following ultraintense laser-pulse interaction with solid targets is discussed.

The experiment was carried out at the VULCAN laser facility, Rutherford Appleton Laboratory (RAL). The proton beams (originating from hydrocarbon impurities located on the target surfaces) were produced by irradiating thin Al foils with a 20 J, 1-ps laser pulse at an intensity of 10^{19} W cm^{-2}. A second laser pulse with the same characteristics was focused onto a separate target, and the protons were used to probe this interaction (see Fig. 1). The delay between the two laser pulses could be varied optically. The angle between proton beam and interaction beam propagation directions was approximately 75°.

The protons were emitted from the rear of the target with small angular divergence (10°–15° half-aperture), cut-off energy of about 10 MeV, and a Boltzmann spectrum with $T \sim 1.5$ MeV. The proton source had an apparent diameter d smaller than 10 μm. This was determined via penumbral edge measurements and imaging of static objects via mul-

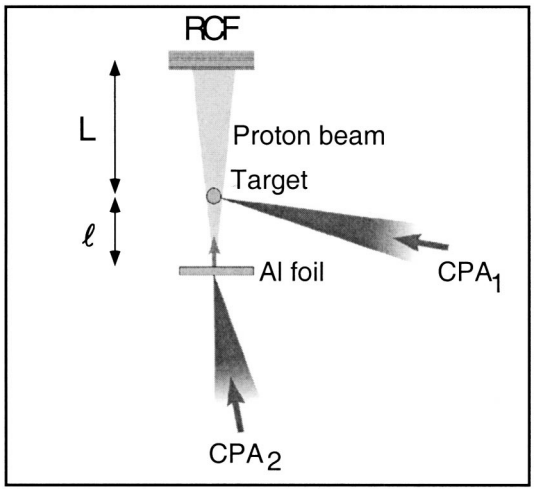

FIG. 1. Experimental arrangement for proton probing of ultraintense laser–target interactions.

[a]Electronic mail: m.borghesi@qub.ac.uk
[b]Present address: Dipartimento di Energetica, Universitá di Roma "La Sapienza", 00161 Roma

tiple scattering. The proton probe was used in a point-projection imaging arrangement with magnification M determined by $M=1+L/\ell$, with $L=2.5$ cm and $\ell=2$ mm, respectively, the object-to-detector and source-to-object distances. The protons were detected using a stack of MD 55-Gafchromic™ radio-chromic films[7,8] (RCF, a dosimetric detector), protected by a 25-μm Al filter. In each RCF, two 15-μm layers of organic dye, separated by about 140 μm, are embedded in 270-μm-thick plastic. The dye reacts to ionizing radiation by changing its optical density. The two active layers can be separated mechanically after exposure.

Since protons deposit energy mainly in the Bragg peak at the end of their range and the number of the protons decreases with their energy, the signal on each active layer is mainly due to protons having energies within a narrow range. At any given distance from the proton beam axis, about 50% of the signal in an active layer is due to protons within an energy range δE_p of the order of 0.5 MeV.

The spatial resolution of the diagnostic is determined by two factors, the size d of the proton source and the width δs of the point spread function of the detector (mainly due to scattering near the end of the proton range). The latter can be determined, via Monte Carlo simulations,[9] to be $\delta s \sim 20$ μm for a proton energy $E_p \sim 7$ MeV. The spatial resolution is therefore of the order of $\Delta s \sim \max(d, \delta s/M)$. For $M>10$, Δs is therefore better than 10 μm.

The ultimate limit of the temporal resolution is given by the duration of the proton burst τ at the source. According to the models,[2] τ is of the order of the laser-pulse duration ($\sim$1 ps). However, in the conditions of the measurements reported here, other effects are dominant. In particular, the finite energy resolution of the active layers and the finite transit time of the protons through the region in which the fields are present limit the resolution to several picoseconds (e.g., 4–5 ps for the layer corresponding to $E_p=7$ MeV).

Energy dispersion provides the technique with an intrinsic multiframe capability. In fact, since the sample to be probed is situated at a finite distance from the source, protons with different energies reach it at different times. As the detector performs spectral selection, each active layer contains, in first approximation, information pertaining to a particular temporal delay.

Under favorable conditions (i.e., when collisional stopping/scattering of the protons in the sample is negligible), this technique showed unique capabilities for the detection of the onset and decay of highly transient electromagnetic fields. In Fig. 2, proton images taken (in a single shot) after ultraintense irradiation of a 50-μm Ta wire are shown. In the earliest frame the proton beam intensity cross section is undisturbed, apart from the collisional shadow of the target and some perturbations visible around the interaction area, due to the plasma created by the pre-pulse. In layers shown in Figs. 2(b) and 2(c), corresponding to proton transit through the target close to the peak of the interaction pulse, the proton beam cross section is modified dramatically. Following the expulsion of hot electrons during the interaction, the wire charges up positively and deflects the protons away from its surface. The charge-up starts between 5 and 10 ps ahead of the peak of the pulse, when the intensity on target

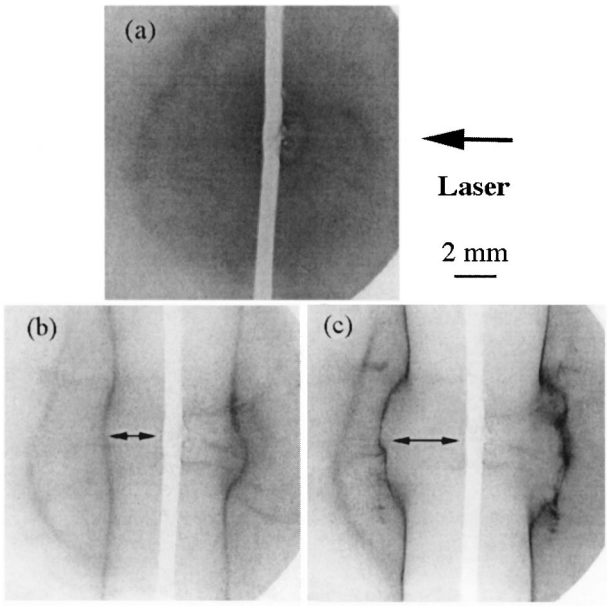

FIG. 2. Proton images taken during laser irradiation of a 50-μm Ta wire. The frames are three active layers from the same shot and refer to different probing times ahead of the peak of the interaction pulse: (a) $E_p \sim 8$ MeV, $\Delta t \sim -12$ ps; (b) $E_p \sim 7$ MeV, $\Delta t \sim -8$ ps; (c) $E_p \sim 6$ MeV, $\Delta t \sim -3$ ps.

due to the rising edge of the pulse[10] can be estimated to be in the 10^{16}–10^{17} W/cm^2 range.

By matching the observed proton deflection to 2-D particle-tracing results, the temporal evolution of target charge and electric field can be inferred. The field at the target surface (at the position indicated by the arrow in Fig. 2) varies between 1.5×10^{10} V/m in Fig. 2(b) and 2.0×10^{10} V/m in Fig. 2(c). After 20–30 ps, no deflection is observed, meaning that the maximum field is less than $\sim 5\times10^{8}$ V/m.

Figure 3 shows proton images taken, again in a single shot, after ultraintense irradiation of a glass microballoon. Even in this case, the protons are deflected away from the

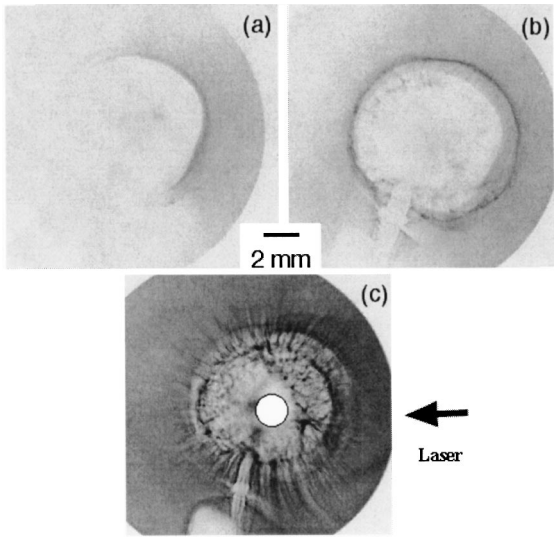

FIG. 3. Proton images taken following laser irradiation of a 150-μm glass microballoon. The original size and position of the target are indicated by the solid circle in Fig. 3(c). Each picture refers to subsequent active layers (i.e., different proton energy E_p and different probing delay Δt from the peak of the interaction pulse): (a) $E_p \sim 8$ MeV, $\Delta t \sim -2$ ps; (b) $E_p \sim 7$ MeV, $\Delta t \sim 1.5$ ps; (c) $E_p \sim 4.5$ MeV, $\Delta t \sim 15$ ps.

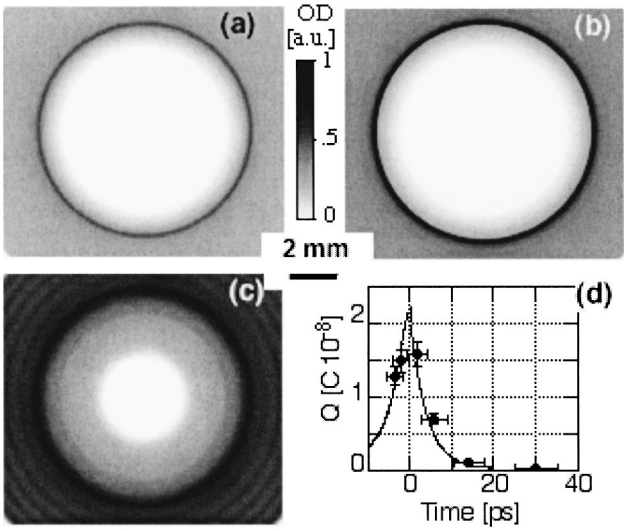

FIG. 4. Particle tracing simulation results. In (a), (b), and (c), the optical density distribution expected in the corresponding detector layers of Fig. 3 after propagation of the proton beam in the field of a discharging microsphere is shown. Distances and dimensions are as in the experiment. The simulation uses the experimental proton spectrum and takes into account the response of each active layer to protons of different energy. Frame (d) shows the charge evolution inferred from electrostatic considerations from the experimental data (points), and the dynamic function used in the simulation (line).

target by an outwardly directed electric field. The experimental deflection can be matched to the predicted deflection for protons propagating in the Coulomb field of a static charge. By using this method, the target's charge, and consequently the electric field near the surface, can be estimated at various times, as shown in Fig. 4(c). By taking, for example, the layer of Fig. 3(c), the deflection is consistent with $Q \sim 1.5 \times 10^{-8}$ C, giving again a field of about 10^{10} V/m near the target surface.

However, associating a single proton energy E_p and, consequently, a time delay t_0 to each layer is only valid in first approximation. In reality, protons with energy higher than E_p will also contribute to some extent to the dose released in the layer, which will also contain information relating to the field distribution at times earlier than t_0. In order to interpret more fully the data of Fig. 3, three-dimensional particle-tracing simulations of proton propagation in the field of a discharging sphere were performed. Simulation results for the various layers are shown in Fig. 4. By reconstructing layer-by-layer the optical density patterns and comparing them with the experimental data, the code (PTRACE) provides more detailed information on the target charge history. The curve plotted in Fig. 4(d) (a Lorentzian before the peak, a decreasing exponential after the peak) was the one that best reproduced the general characteristics of the data (e.g., diameter and thickness of the rings). Modeling of more detailed features of the data is currently in progress.

A simple explanation of the phenomenon observed is as follows: during the interaction, as soon as the intensity is sufficiently high, a population of suprathermal electrons is generated in the interaction region.[1,11,12] Their energy distribution can be described by a Boltzmann exponential, with temperature depending on the instantaneous laser intensity. Due to their kinetic energy, the fast electrons tend to escape from the target, leaving it positively charged. The subsequent fast electron motion is therefore affected by the Coulomb potential of the target. While a fraction of the electrons has enough energy to escape from this potential, lower energy electrons will reach a maximum distance and move back into the target. Estimates for the escaped fraction in conditions consistent with the experimental observations indicate that about 35% of the electrons can escape, while typical return times for the trapped electrons are of the order of a fraction of a picosecond. Therefore, the charge detected in the experiment is only due to the electrons that have escaped the electrostatic potential. The measured charge $Q \sim 10^{-8}$ C corresponds to $\sim 10^{11}$ electrons leaving the target. If one takes 1 MeV as an indicative energy for the escaping electrons, they would carry about 1% of the laser energy. These numbers are consistent with reported experimental measurements.[12]

The target's charge grows as long as the instantaneous laser intensity is increased, since electrons with higher energies are produced and are able to leave the target. The discharge observed following the peak of the interaction pulse is most likely due to charge redistribution in the target and stalk supporting it. The observation of target neutralization via redistribution of charge on such short time scales provides a further example of the fundamental physical processes that can now be investigated using the proton imaging diagnostic.

In conclusion, proton probing techniques have enormous potential for the diagnosis of fundamental physical problems, which were impossible to explore up to now. By using this diagnostic, the measurement of the large, highly transient electric fields due to charging of laser-irradiated targets has been obtained, determining their evolution on a picosecond scale.

We would like to acknowledge the support provided by the staff of the Central Laser Facility at RAL, and discussions with Dr. H. Ruhl (General Atomics). This work has been supported by ESPRC grants.

[1] F. Amiranoff, Meas. Sci. Technol. **12**, 1795 (2001), and references within.
[2] J. T. Mendonça, J. R. Davies, and M. Eloy, Meas. Sci. Technol. **12**, 1802 (2001), and references within.
[3] D. West and A. C. Sherwood, Nature (London) **239**, 157 (1972).
[4] C. W. Mendel, Jr. and J. N. Olsen, Phys. Rev. Lett. **34**, 859 (1975).
[5] J. Cobble, R. P. Johnson, T. E. Cowan, N. Renard-le-Galloudec, and M. Allen, J. Appl. Phys. **92**, 1775 (2002).
[6] M. Borghesi, S. V. Bulanov, D. H. Campbell, R. J. Clarke, T. Zh. Esirkepov, M. Galimberti, L. A. Gizzi, A. J. Mackinnon, N. M. Naumova, F. Pegoraro, H. Ruhl, A. Schiavi, and O. Willi, Phys. Rev. Lett. **88**, 135002 (2002).
[7] A. J. Mackinnon, M. Borghesi, S. Hatchett, M. H. Key, P. Patel, D. H. Campbell, A. Schiavi, R. Snavely, and O. Willi, Phys. Rev. Lett. **86**, 1769 (2001).
[8] W. L. C. McLaughlin, J. C. Humphreys, D. Hocken, and W. J. Chappas, Nucl. Instrum. Methods Phys. Res. A **302**, 165 (1991).
[9] J. F. P. Ziegler, J. P. Biersack, and U. Littmark, *The Stopping and Range of Ions in Solids* (Pergamon, New York, 1996); [http://www.srim.org].
[10] C. Danson, L. Barzanti, Z. Chang, A. E. Damerell, C. B. Edwards, S. Hancock, M. R. Hutchinson, M. H. Key, S. Luan, R. R. Mahadeo, J. P. Mercer, P. Norreys, D. A. Pepler, D. A. Rodkiss, I. N. Ross, M. A. Smith, R. A. Smith, P. Taday, W. T. Toner, K. W. M. Wigmore, T. B. Winstone, R. W. W. Wyatt, and F. Zhou, Opt. Commun. **103**, 392 (1993).
[11] F. N. Beg, A. R. Bell, A. E. Dangor, C. N. Danson, A. P. Fews, M. E. Glinsky, B. A. Hammel, P. Lee, P. A. Norreys, and M. Tatarakis, Phys. Plasmas **4**, 447 (1997).
[12] G. Malka and J. L. Miquel, Phys. Rev. Lett. **77**, 75 (1996).